Searching for Extreme Emission Line Galaxies
In miniJPAS and MUSE HUDF surveys

José M. Vílchez
IAA-CSIC

J. Iglesias-Páramo
I. Del Moral-Castro
A. Arroyo-Polonio
C. Kehrig
A. Lumbreras
I. Breda
. . .



La Cristalera, Miraflores de la Sierra, 4-7 febrero 2024

EXTREME EMISSION LINE GALAXIES – EELG

=> EELG galaxies host ***extreme star formation*** (SF) events. (e.g. GPs) -> provide keys for our understanding of early galaxy evolution.

Ly_C photons leakage from EELGs -> expected **main fraction of the budget for re-ionization** of the Universe
(e.g., Erb+ 2016; Yang+; Sobral+ 2018; Naidu+2022; Matthee+ 2022).

=> EELGs present intense **emission lines** with **Equivalent Widths $EW_o \geq 300$ Å**

Currently **different selection criteria =>** EELGs include different categories:
Green Peas, Blue berries, Xtreme HII galaxies and BCDs, ELDots / Hα Dots…
(e.g. Cardamone+ 2009, Amorin+ 2010; Yang+ 2017; Terlevich+ 1991; Bekki 2015, Salzer+ 2020)

EELGs -> large EW_o([OIII]+H_β) => common **strong *Ly_α*** emission (Tang+2021)
GPs -> ***typical Ly_C leakers*** present also ***high $EW_o(Ly_\alpha)$*** (Izotov+ 2016; 2018)

EELG selection -> blind search for emission line targets -> minimise bias (e.g. in BBand samples)
*Important to **increase EELG samples at the lowest mass, lowest metallicity galaxies** populating this ranges in M_* - Metallcity - SFR and M_* - SFR relations (e.g. Indhal+ 2021; Curti+ 2023).*

SEARCHING FOR EELGs

Currently adopted EELGs selection criteria => a mixed bag of types*:** GPs from broad band photometry (e.g. à la Cardamone+ 2009; van der Well 2011), narrow/medium band imaging (Sobral+ 2014; Lumbreras-Calle+ 2022), spectral targets (e.g. Amorín+ 2015; Maseda+ 2018, Boyett+ 2024 JADES ***JWST/NIRSp; Zou+ 2024 ***DESI*** XMP-ELGs) . . .

We **propose *a selection of EELGs in wide field emission-line surveys*:**
Selecting *galaxies with $EW_o \geq 300$ Å in at last one line* of [OIII]5007, [OII]3727, H_α (Iglesias-Paramo+ 2022).

SEARCH CONDUCTED with:

1.- **JPAS Survey**: MiniJPAS - AEGIS field (Bonoli+ 2021)
Wide-field spectro-photometry in **56 Narrow Band Filters** (Equiv. R~60) sampling a strip of 1^o over the EGS (AEGIS) field (+ SDSS filters).
Search within $0 \leq z \leq 0.8$ (Iglesias-Páramo+ 2022)

Also with:

2.- **DR2 MUSE HUDF Survey**: MOSAIC (9’) + UDF 10 (1’) + MXDF (41”Ø) fields (Bacon+ 2023)
MHUDF survey provides deep spectra + cutouts cubes for each selected candidate

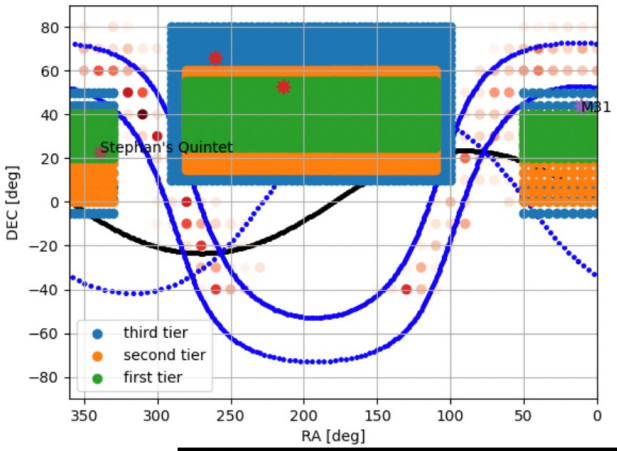
(DR2 -> also incl. catalogue of physical properties for a gal. subsample)

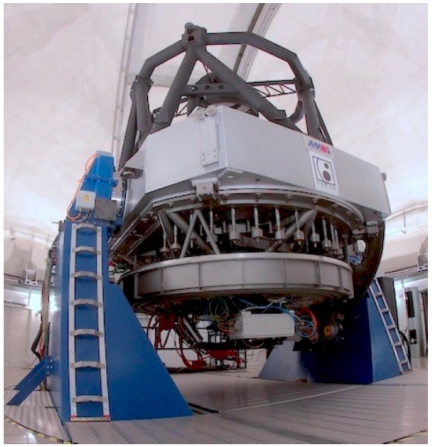
1

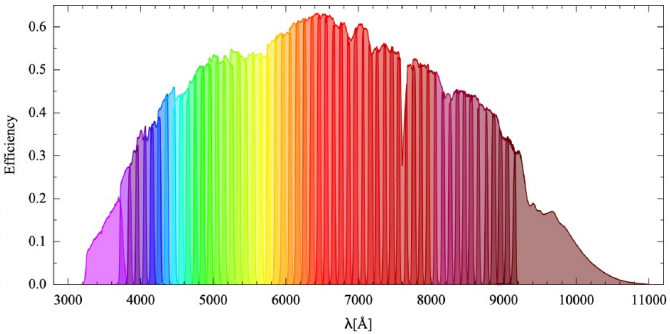
J-PAS

Javalambre Physics of the Accelerating Universe Astrophysical Survey

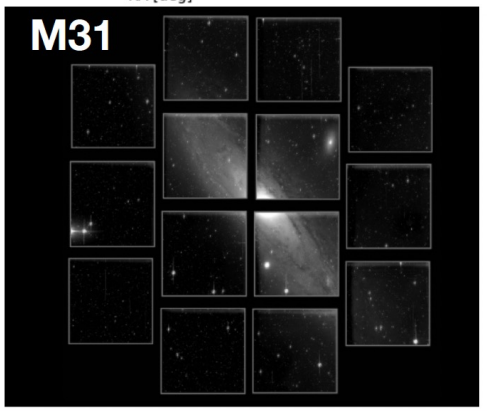
- >5000 deg^2 in the northern sky
- 2.5m telescope at OAJ
- Photometric system: 56 NB; fwhm = 145 Å (R~60)
- Covering every 100 Å the whole optical range
- JPCam: 14 CCDs, FoV~4 deg^2; 0.23 arcsec/pixel

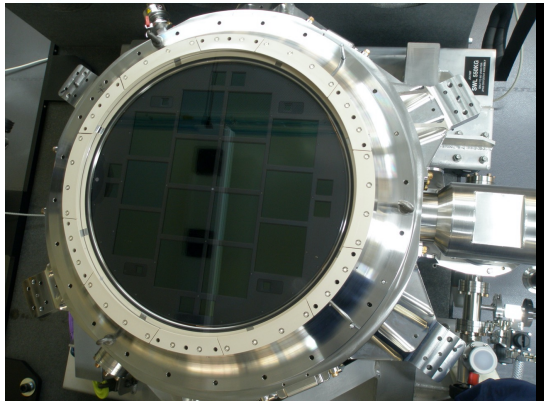


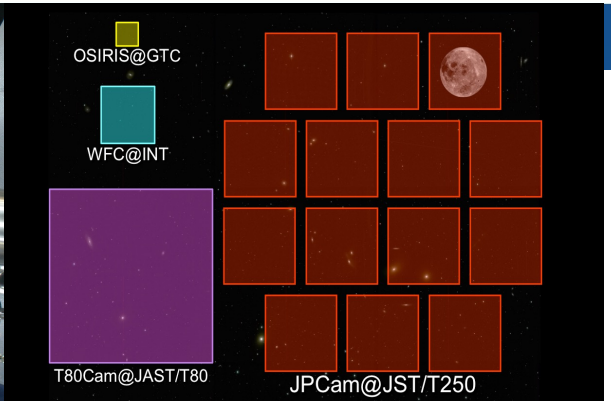




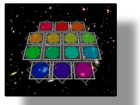
Benítez + 2009; Benítez + 2014
Cenarro + 2014







J-PAS: a survey for Galaxy Evolution



JPCam
O.A. Javalambre

Identification and Characterization of Extreme Emission Line Galaxies-EELGs

A&A 665, A95 (2022)
https://doi.org/10.1051/0004-6361/202243931
© J. Iglesias-Páramo et al. 2022

Astronomy & Astrophysics

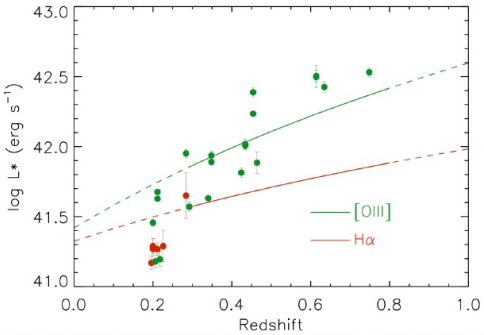
The miniJPAS survey: A search for extreme emission-line galaxies

J. Iglesias-Páramo[1], A. Arroyo[1], C. Kehrig[1], J. M. Vílchez[1], S. Duarte Puertas[16,1], E. Pérez-Montero[1], I. Breda[1], Y. Jiménez-Teja[1], C. López Sanjuan[15], A. Lumbreras-Calle[2], P. Coelho[3], S. Gurung-López[4,5], C. Queiroz[13], I. Márquez[1], M. Pović[17,1], R. González Delgado[1], J. Chaves-Montero[7], D. Sobral[11,12], A. Hernán-Caballero[2], J. A. Fernández-Ontiveros[2], L. A. Díaz-García[1], A. Alvarez-Candal[1,14,6], R. Abramo[3], J. Alcaniz[6], N. Benítez[1], S. Bonoli[7,8,2], A. J. Cenarro[15], D. Cristóbal-Hornillos[2], R. Dupke[6], A. Ederoclite[2], A. Marín-Franch[15], C. Mendes de Oliveira[9], M. Moles[2], L. Sodré Jr.[9], K. Taylor[10], J. Varela[15], H. Vázquez-Ramió[15], and J-PAS team

New methodology to obtain a complete census of EELGs with J-PAS over large areas by detection of galaxies with equivalent widths EW ≥ 300 Å in the emission lines: [O II]λλ3727,3729 Å, [O III]λ5007 Å, and Hα

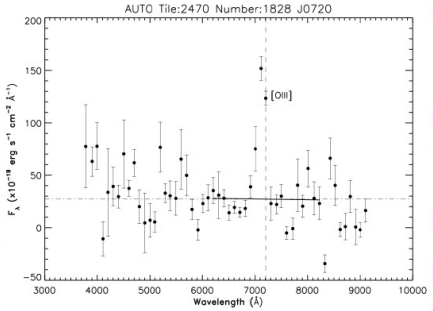
Preparing for the large J-PAS sky coverage

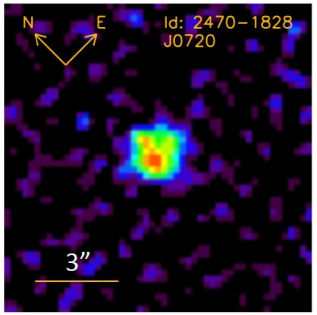
Iglesias-Páramo+ (2022)



Characteristic luminosity L* as a function of redshift (Comparat+ 2016) for [OIII]λ5007Å (solid green) and Hα (solid red) lines.
Filled points correspond to miniJPAS confirmed EELGs (17), id. color code.

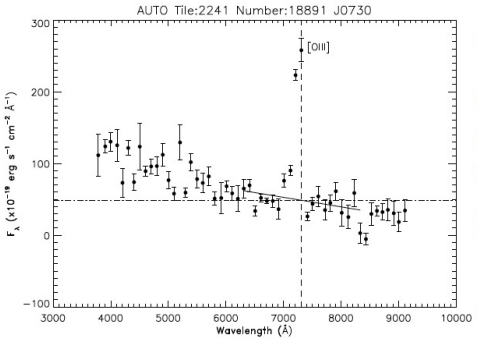
New EELG candidate

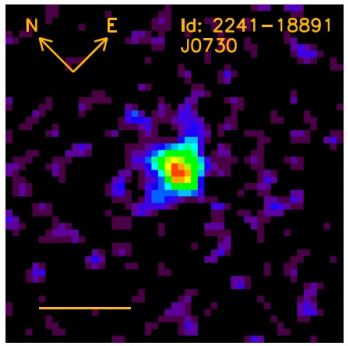


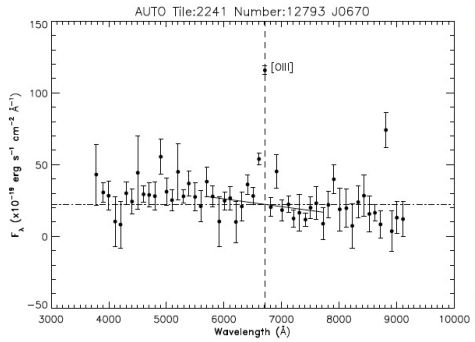


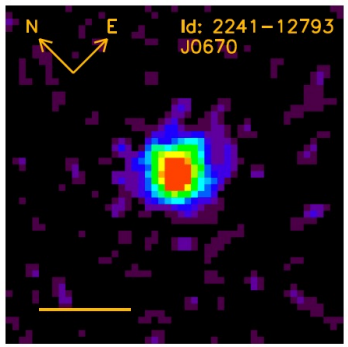
RESULTS: **17 EELGs with EW_0 [OIII]≥300 Å | $0.196 \leq z \leq 0.748$; $20.5 \leq r_{SDSS} \leq 24$ mag**

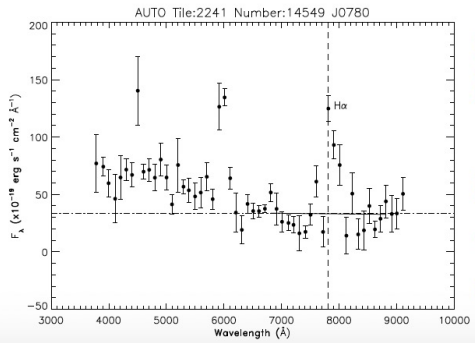
(Examples of) EELG new selections

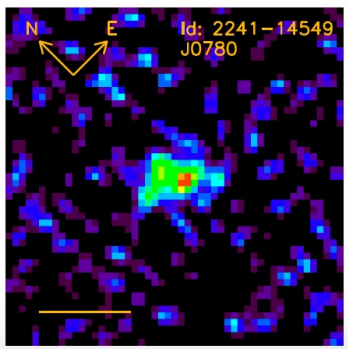












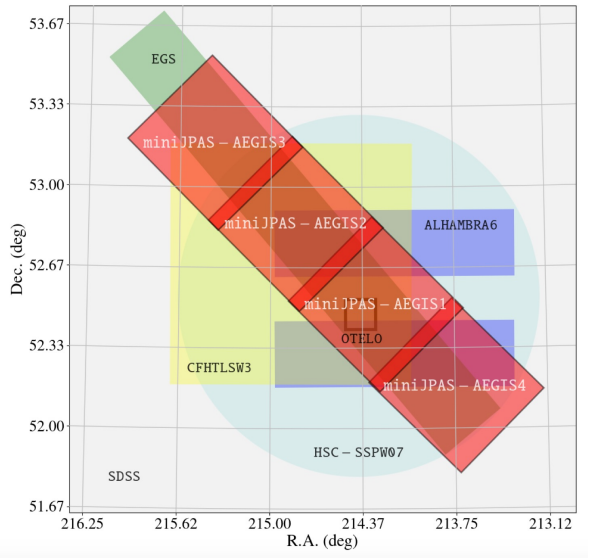
Sample:

17 [OIII] sources peaking

$0.2 \leq z \leq 0.3$

Highest EW_o[OIII] =1758 Å

$41.17 \leq \mathrm{Log(Lum/erg\ s^{-1}}) \leq 44.25$



EELGs sky density consistent w/ previous work:

Lumbreras-Calle+ 2022 JPLUS (Local EELGs $z \leq 0.06$)

Amorin+ 2015 (20k zCosmos bright survey)

JPAS Extreme Emission Line Galaxies properties

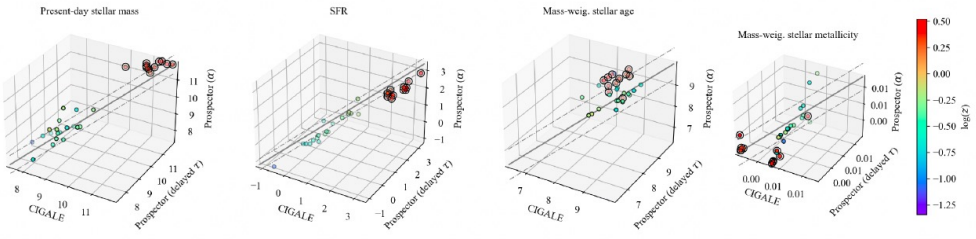
Identification and Characterization of Extreme Emission Line Galaxies-EELGs

Multiwavelength exploration of Extreme Emission Line Galaxies detected in miniJPAS survey

Iris Breda[1], José M. Vilchez[1], Enrique Pérez-Montero[1], Carolina Kehrig[1], Jorge Iglesias-Páramo[1], Antonio Arroyo-Polonio[1], Rosa González Delgado[1], Abramo, R.[2], Alcaniz, J.[3], Benítez, N.[1], Bonoli, S.[4,5,6], Cenarro, A. J.[7], Cristóbal-Hornillos, D.[6], Dupke, R.[3], Ederoclite, A.[6], Hernán-Caballero, A.[7], Marín-Franch, A.[7], Mendes de Oliveira, C.[8], Moles, M.[6], Sodré, L.[8], Taylor, K.[9], Varela, J.[7], Vázquez-Ramió, H.[7], and J-PAS team

MNRAS In press

Multi-wavelength EELGs massive SED fitting pipeline developed



Output: physical characterization of the EELGs miniJPAS sample

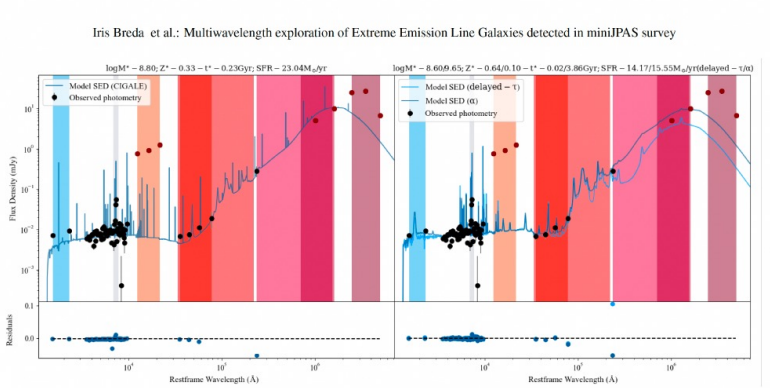
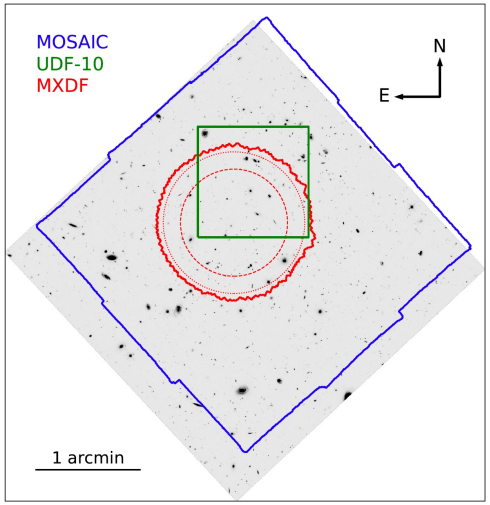


Illustration of the SED fitting results by CIGALE (left-hand side) and Prospector (right-hand side) for the same EELG.
Both, flux density and rest-frame wavelength (Å) are displayed in log scale.

Best-fitting SED models are represented by solid blue lines, observational points are shown by black points and the upper limits by dark red points. The fit residuals are shown in the low panel as well as some derived physical properties presented in the image title.

2 DR2 MUSE HUDF Survey



FIELDS

1. **MOSAIC** → 3´ × 3´ mosaic 9 MUSE fields at a 10-hour depth
2. **UDF-10** -> a single 1´ × 1´, 31-hour depth field
3. **MXDF** (MUSE eXtremly Deep Field) → depth 141 hours. 1' ϕ

Bacon+ (2023)

SEARCH A

EELGs with $EW_o \geq 300$ Å in any one of the lines [OIII]5007, [OII]3727, H_α

Results A: **7 EELGs with robust detection** (5 in [OIII] -one of them also in Hα-, + 2 in Hα only)

In this case we have considered and extended sample from an additional Search 2:

SEARCH B (Extended Sample)

EELGs with **200 Å $\leq EW_o \leq$ 300 Å** in any one of the lines [OIII]5007, [OII]3727, H_α

Results B: **+ 6 EELGs with robust [OIII]5007 detection** (of them: 1 also in [OII]3727; 1 in Hα)

Muse ID	ds name	Ra (deg)	Dec (deg)	z	Line	EWo (Å)	EW (Å)	F (10^{-20}erg s^{-1}cm^{-2})	Log$L$ (erg s^{-1})
(1)	(2)	(3)	(4)	(5)	(6)	(7)	(8)	(9)	(10)
91	MXDF	53.1625	-27.7803	0.719	[OIII]5007	-344.61	-592.38	4098.38	42.82
891	MOSAIC	53.1957	-27.7878	0.2265	Hα	-311.14	-381.62	67945.9	44.04
895	MOSAIC	53.1447	-27.7854	0.2473	[OIII]5007	-362.79	-452.51	92674.08	44.17
					Hα	-331.32	-413.25	57497.73	43.96
2478	MOSAIC	53.1839	-27.7954	0.734	[OIII]4959	-374.78	-649.87	582.64	41.97
					[OIII]5007	-11477.74	-19902.41	2064.91	42.52
2532	MOSAIC	53.1497	-27.8093	0.7525	[OIII]5007	-386.95	-678.12	491.89	41.9
6465	MOSAIC	53.1942	-27.7854	0.7152	[OIII]5007	-362.07	-621.03	668.2	42.03
7373	MXDF	53.1542	-27.7867	0.2759	Hα	-306.61	-391.2	102.29	41.21

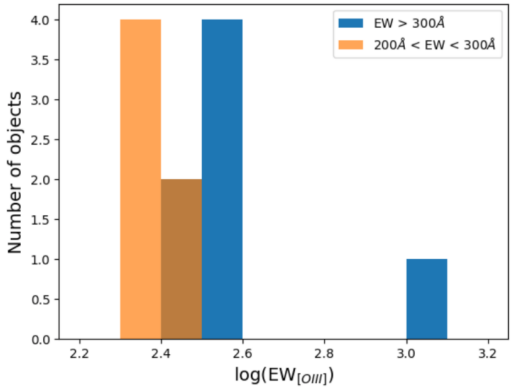
Table 1. Basic properties of the EELG candidates. (1) MUSE source identifier; (2) MUSE data set (MXDF,UDF10 or MOSAIC); (3) Right ascension (J2000.0); (4) Declination (J2000.0); (5) Redshift; (6) Detected emission line with $\geq$ 300 Å; (7) Rest frame equivalent width of the emission feature; (8) Equivalent width of the emission feature; (9) Flux of the emission feature; (10) Luminosity of the emission feature.

1093	MXDF	53.1763	-27.7809	0.5355	[OIII]5007	-235.62	-361.79	5370.59	42.93
1426	MOSAIC	53.1473	-27.8008	0.2799	[OIII]5007	-292.09	-373.84	2485.12	42.6
1561	MOSAIC	53.153	-27.7937	0.7327	[OIII]5007	-253.5	-439.25	1450.04	42.37
1699	MOSAIC	53.154	-27.8052	0.6683	[OIII]5007	-227.63	-379.76	905.36	42.16
6474	MOSAIC	53.1866	-27.7902	0.1239	[OIII]5007	-247.77	-278.47	26043.94	43.62
					Hα	-207.95	-233.72	15342.99	43.39
6865	UDF10	53.1604	-27.7752	0.833	[OIII]5007	-243.93	-447.13	6276.13	43.0
					[OII]3729	-286.38	-694.72	83.74	41.13

Same as Table 1 for the extended sample.

$$41.21\ (41.13) \leq \text{Log(Lum/erg s}^{-1}\text{)} \leq 44.17\ (43.62)$$

$$0.226\ (0.1239) \leq z \leq 0.753\ (0.833)$$



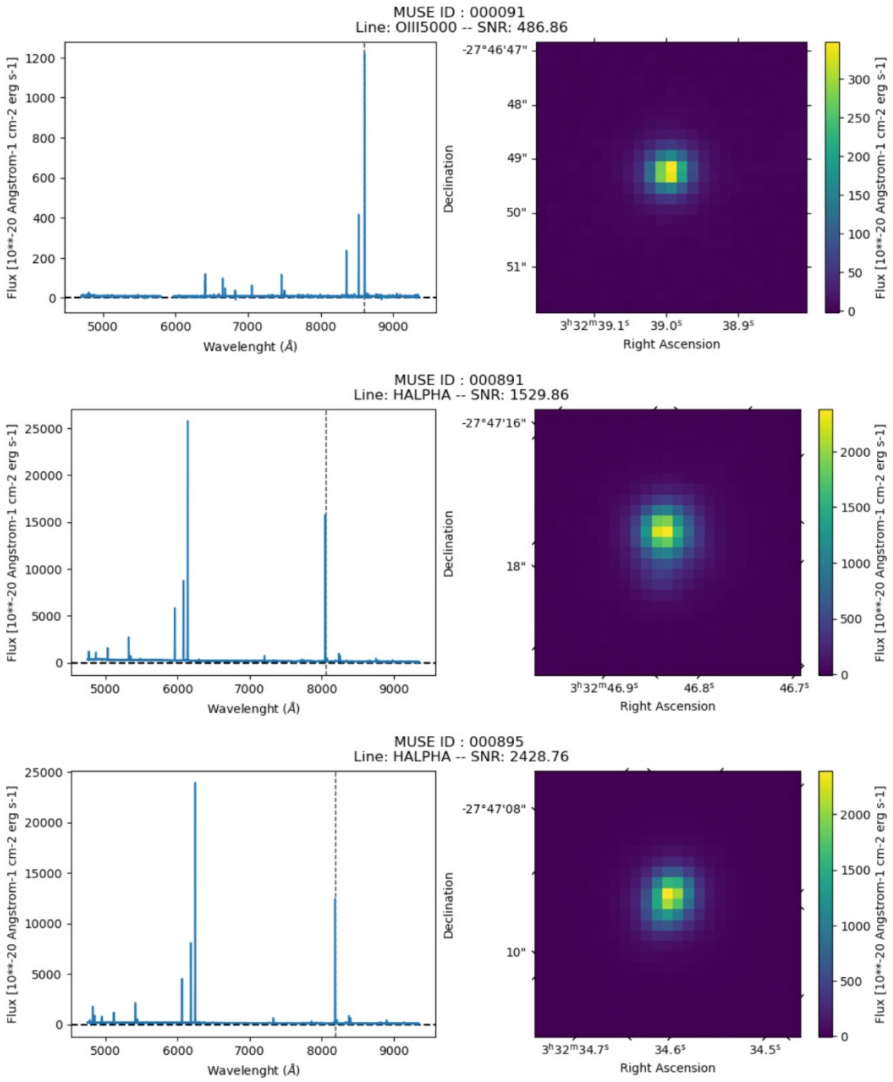
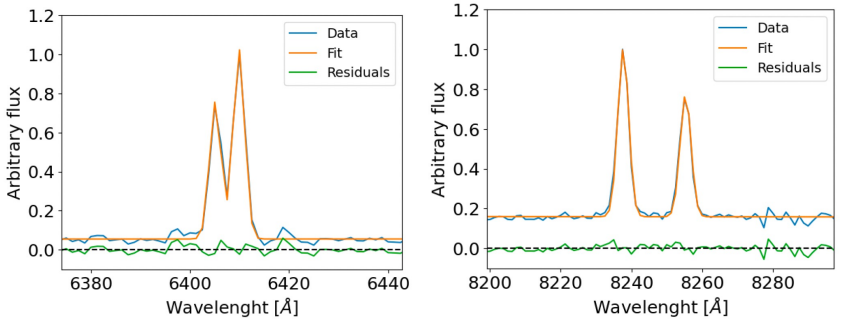
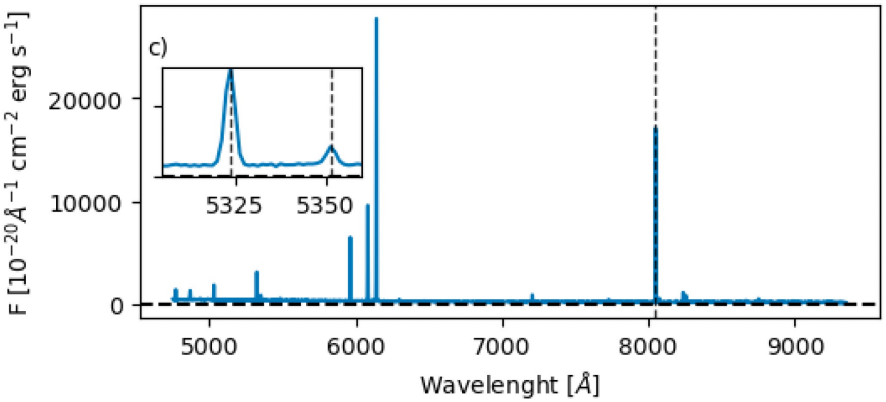


Fig. A.1. Data products from AMUSED for the EELG candidates. *Left:* Spectra using the EMI_ds_id extension. The vertical dashed line indicates the emission line fulfilling our EW0 condition. *Right:* Narrowband source image corresponding to the selection line.


Data
Fit
Residuals
Arbitrary flux
Wavelenght [Å]
Data
Fit
Residuals
Arbitrary flux
Wavelenght [Å]


c)
5325
5350
F [10⁻²⁰ Å⁻¹ cm⁻² erg s⁻¹]
Wavelenght [Å]

EELGs kinematics from MUSE *cutout* cubes

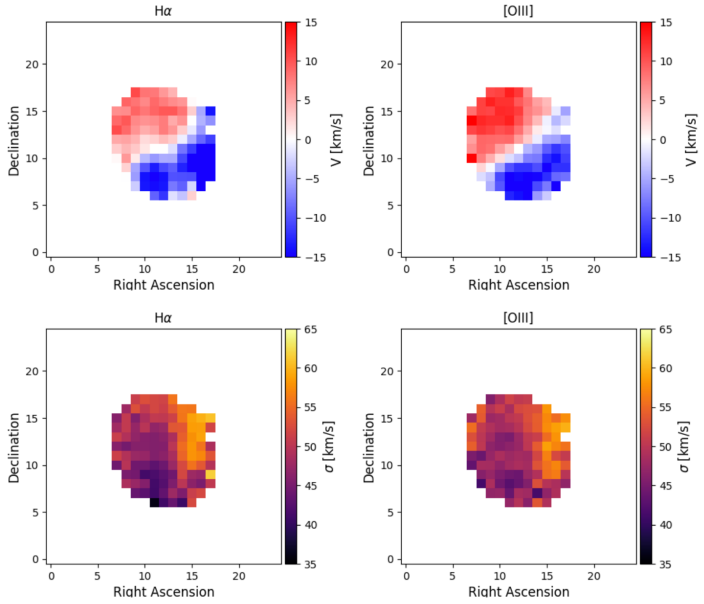


Fig. 1. Kinematics analysis of the Muse ID galaxy 0000891. *Upper left:* Hα rotational velocity. *Upper right:* [OIII] rotational velocity. *Bottom left:* Hα velocity dispersion (σ). *Bottom right:* [OIII] velocity dispersion (σ).

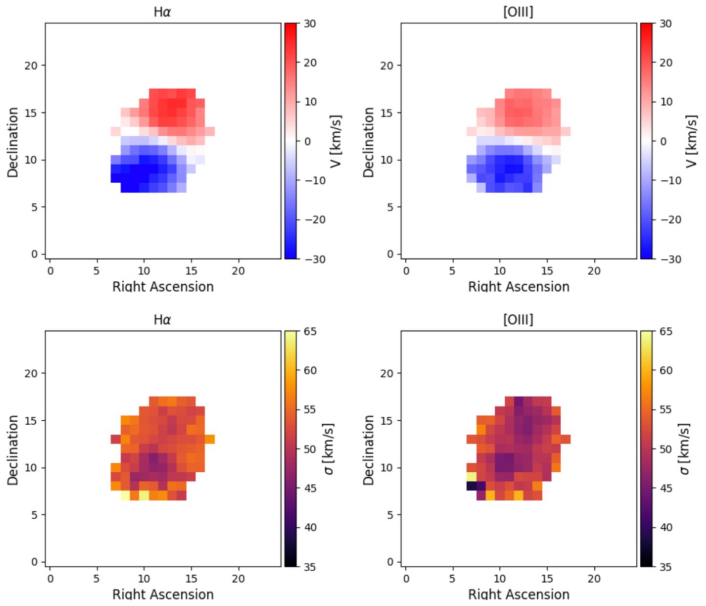


Fig. 2. Same as Fig. 2 for the MUSE ID galaxy 0000895.

Object MOSAIC DR2 ID 000891

Object MOSAIC DR2 ID 000895

=> Low Mass , low Metallicity (e.g. Pilyugin, Vilchez Contini 2004)

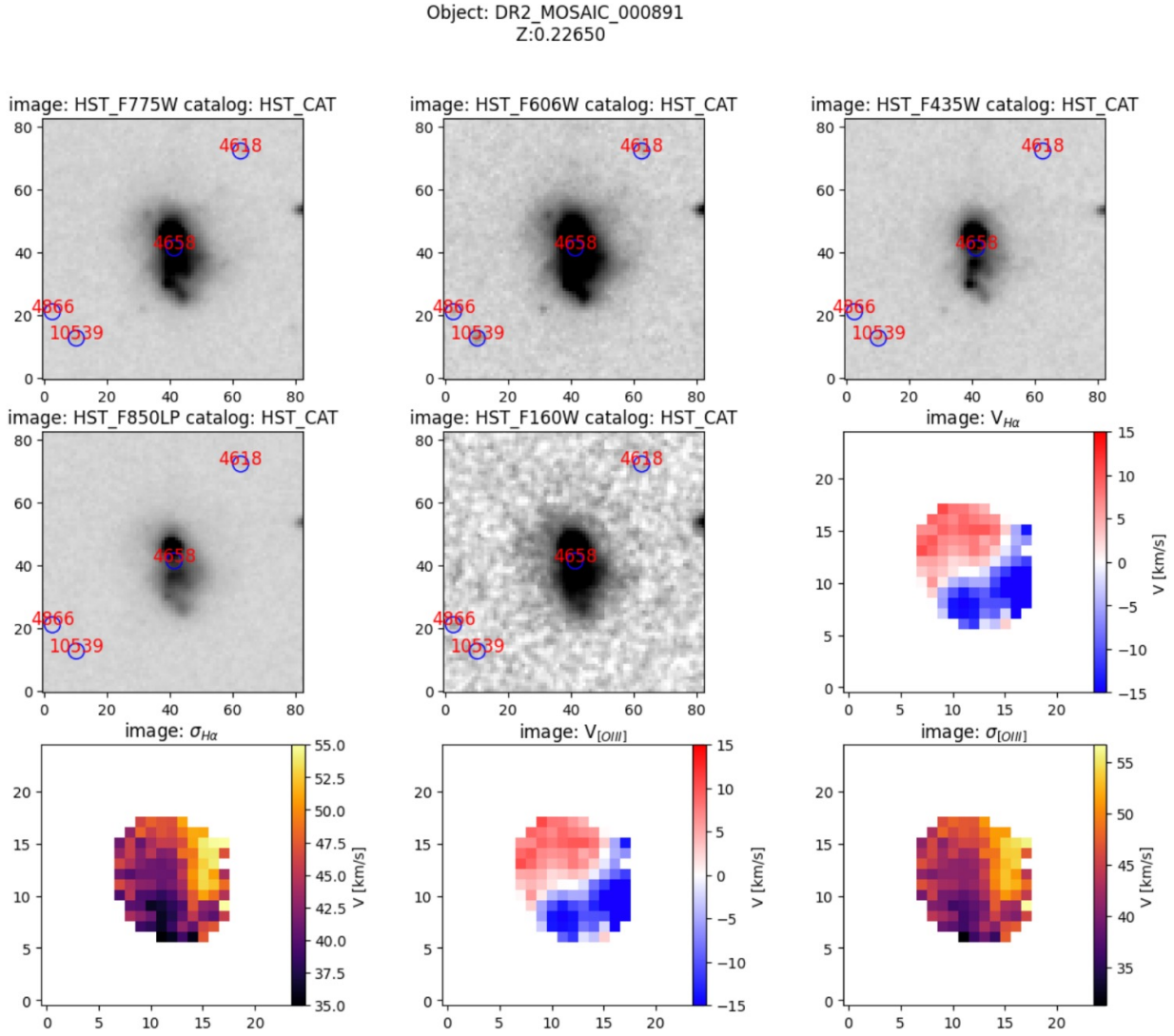
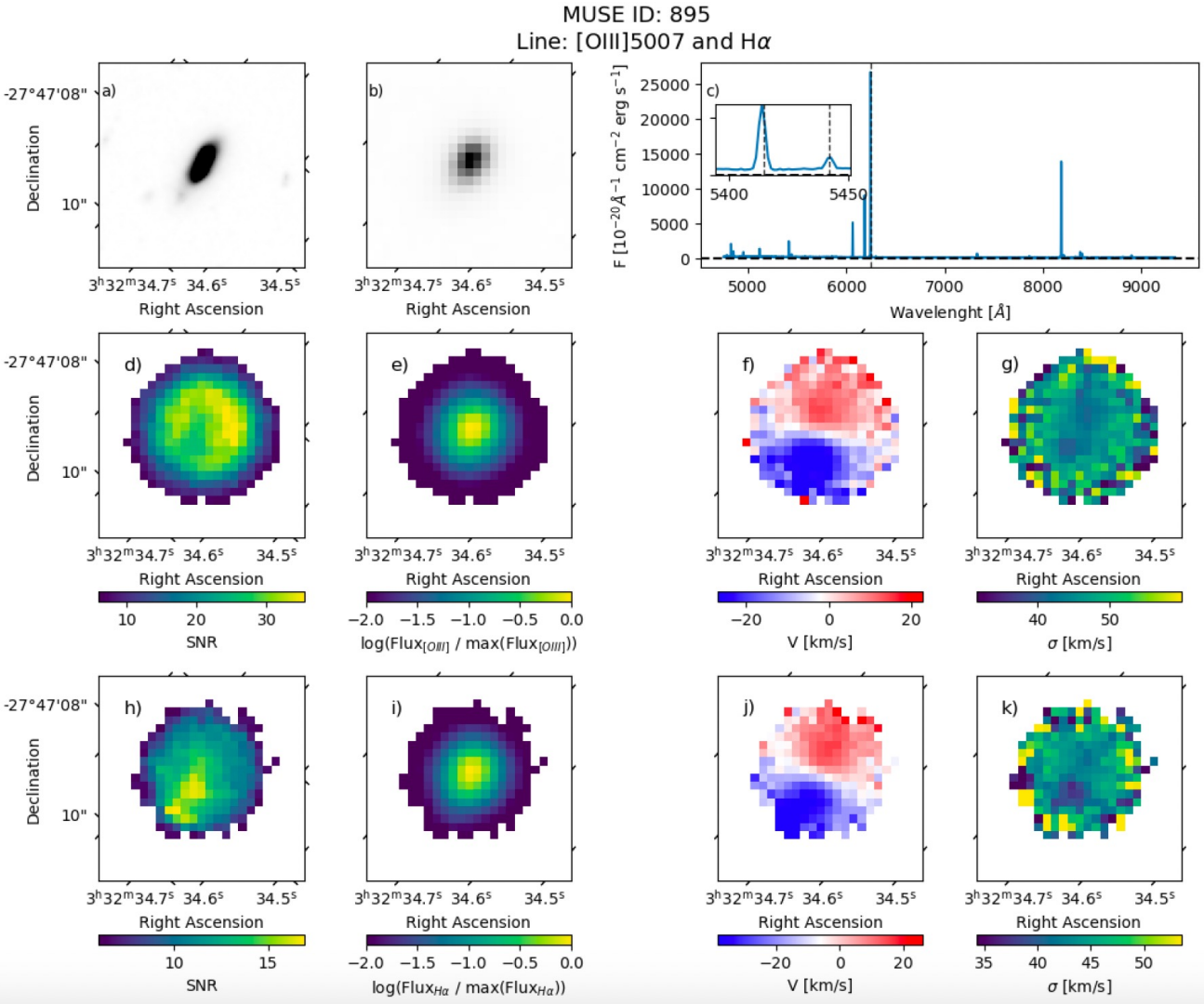

Object: DR2_MOSAIC_000891
Z:0.22650
image: HST_F775W catalog: HST_CAT
image: HST_F606W catalog: HST_CAT
image: HST_F435W catalog: HST_CAT
image: HST_F850LP catalog: HST_CAT
image: HST_F160W catalog: HST_CAT
image: $V_{H\alpha}$
image: $\sigma_{H\alpha}$
image: $V_{[OIII]}$
image: $\sigma_{[OIII]}$
4618
4658
4866
10539
V [km/s]

Fig. 4


MUSE ID: 895
Line: [OIII]5007 and Hα
a)
b)
c)
d)
e)
f)
g)
h)
i)
j)
k)
-27°47'08"
10"
Declination
Right Ascension
3h32m34.7s 34.6s 34.5s
F [10−20 Å−1 cm−2 erg s−1]
Wavelenght [Å]
SNR
log(Flux[OIII] / max(Flux[OIII]))
V [km/s]
σ [km/s]
log(FluxHα / max(FluxHα))

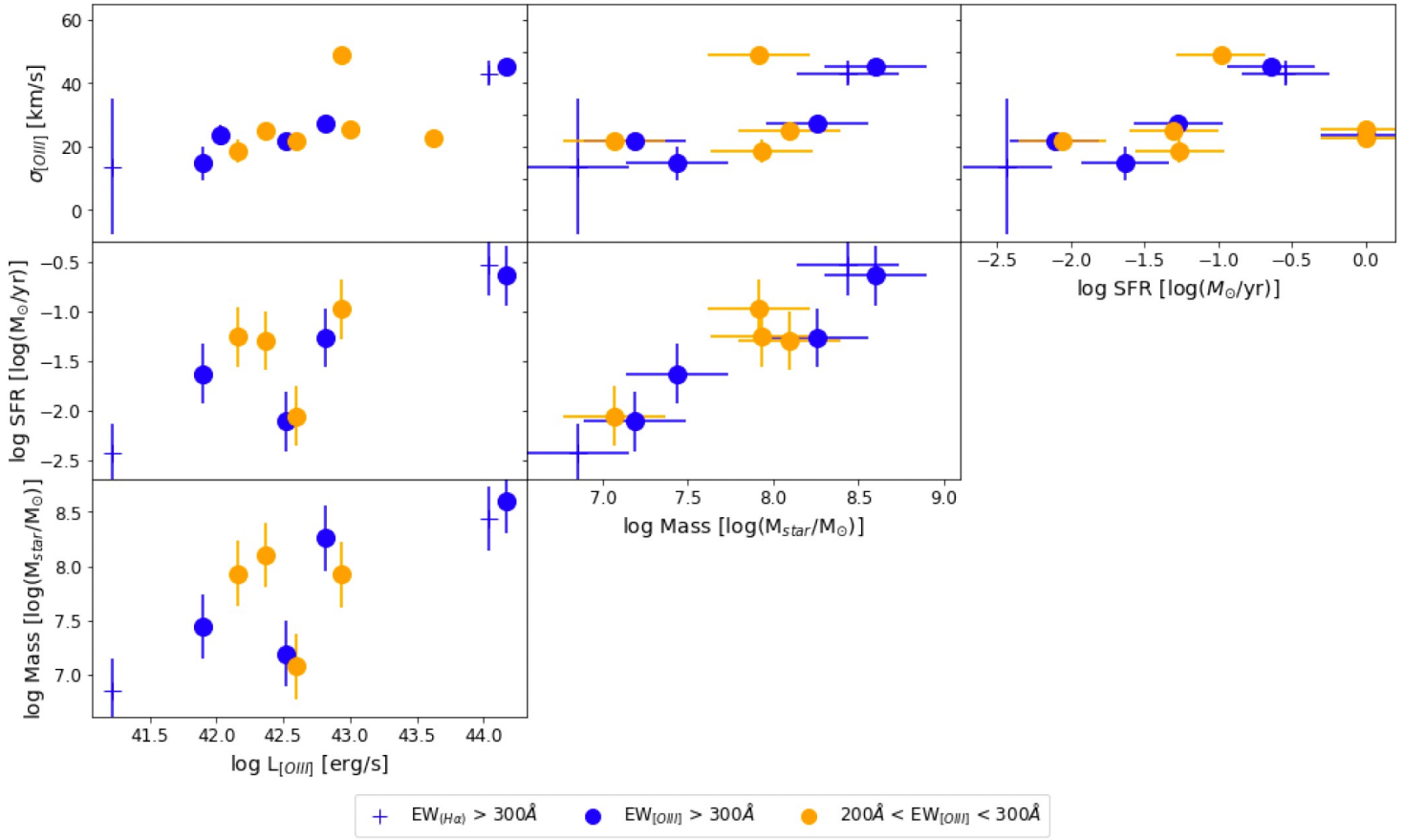


Fig. 4. Correlations between the luminosity, **stellar** mass, star formation rate and $\sigma_{[OIII]}$. We assume typical uncertainties of 0.3dex for mass and star formation rate (see Bacon et al. 2023).

ID	C(Hβ)	Te([OIII]) (10^4 K)	Ne (cm^{-3})	logR_{23} (logO_3)	12+log(O/H)	Notes
91	0.11	1.65±0.04	≤ 50	0.89	7.72±0.03 [7.75]	(b) P
891	0.17	1.45±0.02	73	(0.76)	7.93±0.08	(a) P
895	0.18	1.38±0.01	75	(0.82)	7.99±0.08	(a) P
2478$^{(\star)}$	0.00	1.49±0.20	-	(0.95)	7.89±0.08	(a) P
2532$^{(\&)}$	0.00	-	-	(0.77)	-	(d) P
6465$^{(\star)}$	0.00	-	90	1.03	7.77±0.10	(c) P
7373	0.22	-	-	(0.14)	-	(d) P
1093	0.09	1.31±0.12	≤ 50	0.81	7.90±0.10 [8.05]	(b) E
1426	0.20	-	≤ 50	0.75	7.47±0.10	(c) E
1561	0.13	-	≤ 50	0.83	7.58±0.10	(c) E
1699	0.10	-	544	0.77	7.51±0.10	(c) E
6474	0.13	1.69±0.06	496	(0.83)	7.72±0.08	(a) E
6865	0.12	2.08±0.05	557	0.76	7.38±0.02 [7.37]	(b) E

Table 3. Physical properties and chemical abundances.
($\star$): Hβ flux measurement uncertain.
(&): Only Hβ Balmer line flux measured; C(Hβ)=0 assumed.
Notes (Column 7).-
(a): Oxygen abundance derived from Te([OIII]) following Amorín et al. (2015) relation; expected ±0.08 dex statistical error.
(b): Oxygen abundance from the direct method; the abundance derived using (a) is also given in [ ] for comparison.
(c): Oxygen abundance from R_{23} empirical calibration (Izotov et al. 2019; Williams et al. 2023); expected ±0.10 dex statistical error.
(d): No oxygen abundance derived; only [OIII] nebular line measured.
P: primary EELG sample; E: extended EELG sample.

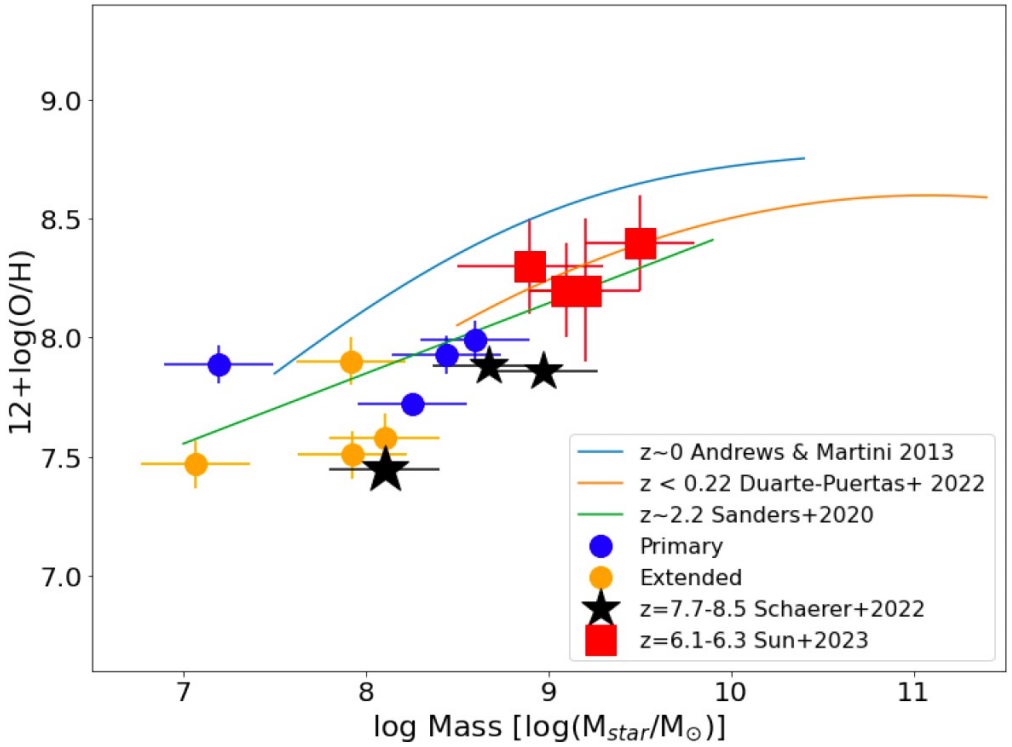


Fig. 6. Mass-metallicity relation. Oxygen chemical abundance and stellar mass for the galaxies in the primary (blue circles) and extended (orange circles) samples in this work, compared to mean relations observed at z~0 (Andrews & Martini 2013), z<0.22 (Duarte Puertas et al. 2022), and z=2.2 (Sanders et al. 2016). Black stars and red squares show recent results for high-redshift galaxies from JWST data (Schaerer et al. 2022; Sun et al. 2023).

Summary of Results

→ **miniJPAS: 17 EELGs with EW_o [OIII]≥300 Å**

$0.196 \leq z \leq 0.748$ | $20.5 \leq r_{SDSS} \leq 24$ mag | $41.17 \leq$ Log(Lum/erg s^{-1}) ≤ 44.25

→ **MHUDF: 7** *(+6)* **EELGs with EW_o [OIII]≥300 Å** *(200 Å $\leq EW_o \leq$ 300 Å)*

0.226 (0.123) $\leq z \leq$ 0.753 (0.83) | $41.21\ (41.13) \leq$ Log(Lum/erg s^{-1}) $\leq$ 44.17 (43.62)

→ **Also: very productive preliminary search for Xtreme Ly$_\alpha$ emitters in MHDF**

→ **Proposal: enlarge statistics for current EELGs/LAEs samples via wide-field emission-ine surveys**

[e.g. JPAS in 2 years could increase EELGs current samples by up to x 1000]


THANKS !
Gracias!

This research has been funded by grants
PID2022-136598NB-C31, C32, and C33

The wokshop has been funded by grant
PID2019-107408GB-C41

all grants are funded by
MCIN/AEI/10.13039/501100011033 and by "ERDF A way of making Europe"